Multiscale mechanical modeling of paperboard

For in-plane uniaxial tensile loadings

Master's Dissertation by

Gustav Boman

Supervisors:
Erik Bergvall, PhD. Tetra Pak Packaging Solutions AB
Eric Borgqvist, PhD. Tetra Pak Packaging Solutions AB
Matti Ristinmaa, Prof. Division of Solid Mechanics

Examiner:
Mathias Wallin, Prof. Division of Solid Mechanics

Preface

I want to express my appreciation and gratitude towards my supervisors at Tetra Pak; Erik Bergvall and Eric Borgqvist. I am very thankful for your patience with my many questions and the solid support you have given me throughout the project. You have been excellent supervisors.

I also thank my supervisor Matti Ristinmaa at the division of Solid Mechanics. Thanks for the advice you have given me and the fruitful discussions we have had throughout the project.

Next, I will thank Frank Ehrhart at Altair Engineering Inc. I highly value the support you have given me in order to get Multiscale Designer to work and perform as intended. Without your crucial help, this work would have been extremely difficult to carry through.

Last, but not least, I like to thank my family members and friends. Thanks for all the support you have given me, not only during my work with this thesis, but also throughout my university studies. I would not have reached this far without you.

Gustav Boman, 15th June 2022

Abstract

This thesis considers an investigation into the possibilities of creating a reasonably accurate multiscale material model for paperboard, with geometry based on X-ray scans of small paperboard samples. The modeling takes place in the software Multiscale Designer by Altair Engineering Inc. A representative volume element (RVE) is used to capture the X-ray geometry and represent macroscopic mechanical properties. The RVE consists of fiber and air phases, perfect fiber-fiber bonding assumed, where the fiber phase is assigned transversely isotropic linear elasticity and isotropic hardening plasticity. This model is considered to behave consistently across different tested X-ray geometries. The results show that it is possible to achieve a reasonably good model fit for in-plane uniaxial tensile tests in MD, CD and 45 degree loading directions.

Further, the model is also exported as a user material in Abaqus, where simulations are performed to compare the multiscale model with a previously established continuum based model. Although the simulation results do not agree completely, there are some similarities, which is promising for further model development.

The multiscale modeling workflow can be automatized to some degree. For this, one needs to ensure the correct content and format of text files used as input in the modeling analyses.

The model may be further developed with additional features such as fiber-fiber bonds, and calibrated towards other and more complex load cases.

Keywords: *paperboard, micromechanics, multiscale, fiber, X-ray, RVE.*

Contents

1   Introduction

Paperboard is a material widely used for packaging food and beverage, with hundreds of billions of paperboard based packages being produced every year. With such high production volumes, it is very important to increase the sustainability of the production; to reduce consumption of raw material and energy. It is equally important to ensure the durability of paperboard throughout its life cycle, including

- Forming of packages, when a consistent behavior during creasing and folding is desired

- Transport and stacking of packages, when compressive stiffness is crucial

- Consumer use, when packages must stay intact to avoid leaking of the contents

Meeting both sustainability and durability requirements is challenging due to the natural variability in mechanical properties of paperboard fibers, making it difficult to accurately predict local material damage and failure. The variability arises from many factors: length, width, thickness, bend and orientation of fibers, the type and age of wood used for extraction, as well as the position of extraction within the wood. Experimental tests can to some extent capture such phenomena, but it can be difficult to draw conclusions from the tests, and eliminate measuring artifacts, such as erroneous adhesive tractions captured in a shear loading experiment.

As an alternative to experiments, virtual models are a great tool to better understand the mechanical behavior of paperboard, and can yield valuable predictions of the response in complex load cases. It is particularly desirable to predict how the mechanics and physics of the material microstructure affect the macroscopic behavior. This necessitates a material model on a microscopic scale. As experimental data from microscale tests is not yet widely available, micromodels are difficult to evaluate. There is, however, a lot of experimental data at a macroscopic level to evaluate micromodels against. Thus one may use a multiscale modeling approach, predicting the macroscopic response based on a micromechanical model. In this work, such an approach is used in the software Multiscale Designer, developed by Altair Engineering Inc. Thanks to a model order reduction implemented in Multiscale Designer, multiscale models can be resolved at the micro scale at a reasonable computation effort.

To accurately formulate a multiscale paperboard model, the microstructure of paperboard must be considered. For this, imaging techniques, such as X-rays, can yield a very accurate representation of the real geometry. In this work, such scans are used as a base for a micromechanical material model.

1.1 Problem Formulation

The aim of this thesis is to investigate the possibilities of creating a reasonably accurate multiscale material model for paperboard, with geometry based on X-ray scans of small paperboard samples. The model is to be calibrated and evaluated at a macroscopic scale. If a reasonably accurate model can be created, its abilities and limitations will be discussed, and the modeling workflow will be determined. These objectives are fulfilled by answering the following questions:

- Can a multiscale, X-ray scan based paperboard model capture the real material response to uniaxial loadings?

- Is the model behavior consistent for different model geometries?

- Can a multiscale modeling workflow be established? If so, which aspects of the workflow are important to consider?

1.1.1 Delimitations

The scope of this work is delimited in the following ways:

- The model aims to capture the response of in-plane uniaxial tensile loadings. Only mechanical loads are considered.

- A single-layer geometry is considered.

- The model captures elastoplastic damage. Other paperboard characteristics, such as dependency on moisture, temperature and strain rate, are not considered.

- Fibers are the smallest considered geometrical entities. No consideration is taken for the physics occurring at lower scales, i.e. the behavior of microfibrills or cellulose molecules.

1.2 Related Previous Work

In recent years, micro-mechanical modeling of paperboard has gained popularity. Some previous works investigate how the response of a fiber network depends on the characteristics of individual fibers (such as length, cross section shape, bend and stiffness), and fiber-fiber bonds (such as bonding area and bond strength reduction during debonding). For such purposes, the fiber network has been manually generated, with fibers with different properties, such as length and orientation, where these properties are generated either randomly or according to some statistical distribution. Previous attempts have also been made at describing the macroscopic behavior with a representative volume element (RVE) ([1], [2]). In particular, [2] used a 1 mm^3 RVE with 10×10×10 elements, with each element being 159×159×40 µm^3. Despite relatively few elements and coarse

resolution, this proved successful for their applications. Still, material parameters for fibers' nonlinear behavior or the fiber bonds are yet to be fully determined.

2 Theory

In this section, the basic mechanics and physics of paperboard is presented. Then an introduction to multiscale modeling is given, followed by a description of the the application of multiscale modeling for paperboard. Next, an overview is presented for the multiscale modeling taking place in Multiscale Designer. This is split into linear and nonlinear material characterizations, where the latter includes a model order reduction. Lastly, some brief words are given on the integration of a multiscale material into CAE interfaces, such as Abaqus.

2.1 Paperboard Physics

Paperboard is a highly anisotropic material. This behavior stems from the manufacturing procedure where cellulose fibers are sprayed on a rolling web, thus creating fiber layers stacked on each other. Most of the fibers are aligned mainly in the longitudinal, machine direction (labeled MD), while some are aligned mainly in the cross direction (CD). The stacking occurs in the thickness direction (ZD). Orthotropy is commonly assumed, defined with aforementioned directions, depicted by Figure 1. Compared to metals, plastics and other industrial base materials, the degree of orthotropy is remarkably large. The stiffness along MD is typically 2-3 times larger than along CD, and typically 100 times larger than along ZD. Fibers and air are the main constituents of paperboard, with starch and other chemicals added. It is mainly the fibers which contribute to the stiffness of the paperboard. Typically the overall density is 300-900 kg/m^3.
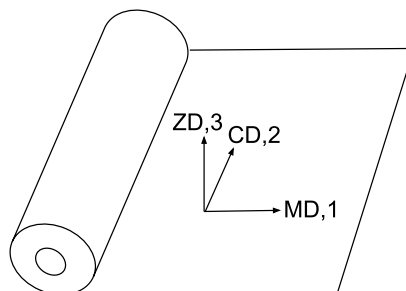

Figure 1: Main orthogonal directions defined for paperboard.

Paperboard possesses a large bending stiffness, making it suitable as a packaging material. A multi-ply structure is often used, where a thick and weak middle ply is surrounded by thin and stiff outer plies, distributing the stiffness towards the edges of the structure, similar to an I-beam. Thus a high ratio of bending stiffness to material use is achieved.

Paperboard is remarkable in its multi-physics behavior, including anisotropy, plasticity, damage evolution as well as dependency on load rate, loading history, temperature and moisture. These characteristics are crucial to consider when formulating material models. The large degree of anisotropy is perhaps the most important feature to capture in models. Upon a closer examination, one sees that paperboard is a highly heterogeneous material with different composition and structure at multiple length scales. The multi-physics behavior can be derived from these heterogeneities, and the relation between them. The scales range from the macroscopic sheet scale down to the microscopic cellulose scale, as seen in Figure 2. To increase model accuracy, one must consider the mechanics and physics taking place at smaller length scales.

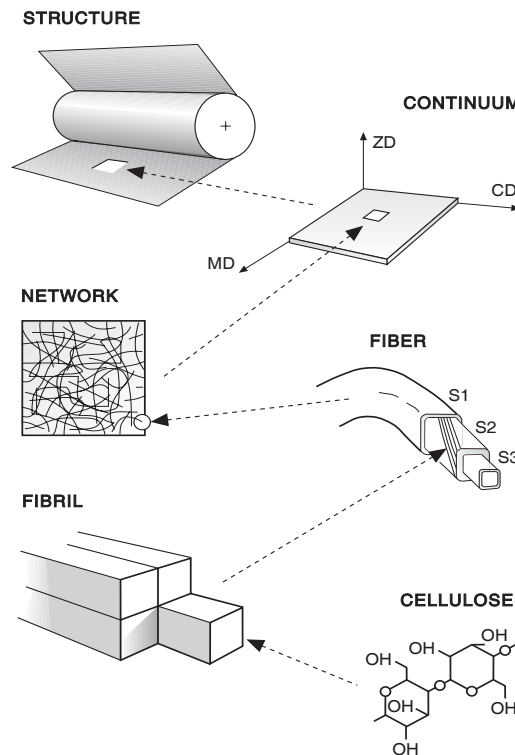Figure 2: Composition and structure of paperboard at different length scales [3].

Increasing model resolution is possible thanks to today's high computation power and methods of accurately reducing model orders, and thus also computation effort. In recent studies, Models of individual fibers and fiber networks have been formulated. Isotropic hardening is commonly used, with some attempts of even more complex models,

e.g. orthotropic plasticity in [4]. A few model proposals are shown in Table 1.

Table 1: Material models for paperboard fibers, as proposed in literature.

Author(s)	Linear model type	Nonlinear model type
Borodulina et al 2016 [5]	Isotropy	Isotropic hardening (bilinear SS-curve)
Brandberg et al 2020 [6]	Transverse isotropy	Linear elastic
Persson 2000 [4]	Transverse isotropy	Orthotropic hardening
Nygårds & Bonnaud 2010 [2]	Isotropy	Isotropic & kinematic hardening
Brandberg & Kulachenko 2017 [7] and 2020 [8], Brandberg et al 2020 [6]	Isotropy	Isotropic hardening (bilinear SS-curve)

2.2   Introduction to Multiscale Modeling

In many industries of today, it is ubiquitous to use composite materials, such as fiber reinforcements, multi-layers, weaves and lattices. Composites include different submaterials (denoted "phases") with desirable mechanical or physical properties, to obtain improved overall behavior. A problem of significant industrial interest is to compose and structure a composite, with certain mechanical and physical properties of included phases, such that a target macroscopic behavior is achieved. For instance, multiscale models have been used to predict failure in carbon fiber composites used in the airplane industry [9]. As phases of composites commonly are dimensioned at the micro scale, a micromodel of the composite is necessitated. As a compromise between model accuracy and computation effort, geometries of these micromodels are as coarse and large-scaled as possible while still capturing the macroscopic material behavior. The geometries are commonly square or rectangular, and either of two types:

- Unit cell, with periodic geometry, as found in e.g. continuous fiber reinforcements.

- Representative volume element (RVE), with non-periodic geometry. This geometry can capture more complex structures, such as non-periodic granular materials. In theory, there is no limitations for the RVE geometry.

The unit cell or RVE is discretized into finite elements, and each phase is assigned a material model based on experiments performed on said phase. To validate the composite model, available experimental data for the total composite is used. As this data is predominantly captured at a macro scale, a multiscale model, connecting micro and macro scale mechanics, is necessitated. The connection between length scales is defined by two processes: homogenization, where large scale mechanics are derived based on smaller scale mechanics, and localization, where small scale mechanics are

derived based on larger scale mechanics. Homogenization is commonly performed as a spatial average up to a larger scale. Localization, however, is a non-trivial task. Clever localization methods have to the potential to reduce the model complexity, and therefore also computation effort. This may make it feasible to run simulations which are too computationally demanding using other methods.

2.3   Basic Multiscale Modeling of Paperboard

To use paperboard in a multiscale modeling framework, both the microstructure and micromechanics of paperboard needs to be captured. The microstructure can be represented very accurately with an X-ray image. As this microstructure is clearly unperiodic, an RVE is to be chosen over a unit cell. As paperboard fibers are typically tens of micrometers wide and thick, the X-ray resolution needs to be smaller than this to capture individual fibers and avoid undesired material homogeneity. The RVE size, i.e. the amount of finite elements for a given resolution, may be chosen as a compromise between computation accuracy and effort. Then, the anisotropic behavior can be captured by dividing the RVE into two phases, fiber and air, and assign an appropriate anisotropic model for the fiber phase. Increasing model complexity, one might also consider a third phase of fiber-fiber interfaces, as the bonding and sliding between fibers heavily influence the macroscopic behavior. For this, cohesive elements and surface interactions may be applied.

To expand the model, one may also consider other mechanical aspects of paperboard, such as dependency on load rate, temperature and moisture. This is achieved with more complex material models assigned to the RVE phases.

2.4   Multiscale Modeling in Multiscale Designer

The modeling in Multiscale Designer is structured into two steps: linear and nonlinear material characterizations. In these steps, linear and nonlinear material models, with corresponding parameter values, are assigned for each phase included in the RVE. Virtual simulations can be performed to calibrate the multiscale material towards experimental data. With both steps completed, the multiscale material can be exported to an external CAE interface. What follows next is the detailed description of each characterization step, and some brief words on the material model export.

2.4.1   Linear Material Characterization

In this step, we compute linear material parameters for the RVE, and thus also for the macroscale material. A linear stress-strain relation holds

$$
\underbrace{\begin{bmatrix} \sigma_{11} \\ \sigma_{22} \\ \sigma_{33} \\ \sigma_{12} \\ \sigma_{13} \\ \sigma_{23} \end{bmatrix}}_{\sigma} = \underbrace{\begin{bmatrix} C_{11} & C_{12} & C_{13} & C_{14} & C_{15} & C_{16} \\ C_{21} & C_{22} & C_{23} & C_{24} & C_{25} & C_{26} \\ C_{31} & C_{32} & C_{33} & C_{34} & C_{35} & C_{36} \\ C_{41} & C_{42} & C_{43} & C_{44} & C_{45} & C_{46} \\ C_{51} & C_{52} & C_{53} & C_{54} & C_{55} & C_{56} \\ C_{61} & C_{62} & C_{63} & C_{64} & C_{65} & C_{66} \end{bmatrix}}_{C} \underbrace{\begin{bmatrix} \varepsilon_{11} \\ \varepsilon_{22} \\ \varepsilon_{33} \\ \varepsilon_{12} \\ \varepsilon_{13} \\ \varepsilon_{23} \end{bmatrix}}_{\varepsilon}
$$

for stresses σ, strains ε and stiffness matrix C. Six finite element simulations of the RVE are performed, based on the chosen material models for each RVE phase. Each simulation has different normalized strain boundary conditions, the only nonzero strain components being

$$\text{BC 1: } \bar{\varepsilon}_{11} = 1, \qquad \text{BC 2: } \bar{\varepsilon}_{22} = 1, \qquad \text{BC 3: } \bar{\varepsilon}_{33} = 1,$$

$$\text{BC 4: } \bar{\varepsilon}_{12} = 1, \qquad \text{BC 5: } \bar{\varepsilon}_{13} = 1, \qquad \text{BC 6: } \bar{\varepsilon}_{23} = 1$$

where $\overline{(\cdot)} = \frac{1}{V} \int_V (\cdot) dV$ denotes spatial normalization over the volume of the RVE. With the FE simulations, normalized stresses $\bar{\sigma}$ are yielded. This in turn yields the stiffness matrix C. For instance, the first column of C is yielded by boundary condition 1

$$
\underbrace{\begin{bmatrix} \bar{\sigma}_{11} \\ \bar{\sigma}_{22} \\ \bar{\sigma}_{33} \\ \bar{\sigma}_{12} \\ \bar{\sigma}_{13} \\ \bar{\sigma}_{23} \end{bmatrix}}_{\bar{\sigma}} = \begin{bmatrix} C_{11} & C_{12} & C_{13} & C_{14} & C_{15} & C_{16} \\ C_{21} & C_{22} & C_{23} & C_{24} & C_{25} & C_{26} \\ C_{31} & C_{32} & C_{33} & C_{34} & C_{35} & C_{36} \\ C_{41} & C_{42} & C_{43} & C_{44} & C_{45} & C_{46} \\ C_{51} & C_{52} & C_{53} & C_{54} & C_{55} & C_{56} \\ C_{61} & C_{62} & C_{63} & C_{64} & C_{65} & C_{66} \end{bmatrix} \begin{bmatrix} 1 \\ 0 \\ 0 \\ 0 \\ 0 \\ 0 \end{bmatrix} = \begin{bmatrix} C_{11} \\ C_{21} \\ C_{31} \\ C_{41} \\ C_{51} \\ C_{61} \end{bmatrix} \implies \begin{bmatrix} C_{11} \\ C_{21} \\ C_{31} \\ C_{41} \\ C_{51} \\ C_{61} \end{bmatrix} = \begin{bmatrix} \bar{\sigma}_{11} \\ \bar{\sigma}_{22} \\ \bar{\sigma}_{33} \\ \bar{\sigma}_{12} \\ \bar{\sigma}_{13} \\ \bar{\sigma}_{23} \end{bmatrix}
$$

Given C elements, stiffnesses and Poisson ratios for the RVE, and thus the macroscale material, are easily yielded from the compliance matrix $S = C^{-1}$. As an example, for a transversely isotropic material the format of S is

$$
S = \begin{bmatrix} \frac{1}{E_{22}} & -\frac{\nu_{23}}{E_{22}} & -\frac{\nu_{12}}{E_{11}} & 0 & 0 & 0 \\ -\frac{\nu_{23}}{E_{22}} & \frac{1}{E_{22}} & -\frac{\nu_{12}}{E_{11}} & 0 & 0 & 0 \\ -\frac{\nu_{21}}{E_{22}} & -\frac{\nu_{21}}{E_{22}} & \frac{1}{E_{11}} & 0 & 0 & 0 \\ 0 & 0 & 0 & \frac{1}{2G_{12}} & 0 & 0 \\ 0 & 0 & 0 & 0 & \frac{1}{2G_{12}} & 0 \\ 0 & 0 & 0 & 0 & 0 & \frac{1+\nu_{23}}{E_{22}} \end{bmatrix}
$$

for Young's moduli E_{11} and E_{22}, shear modulus G_{12} and Poisson ratios ν_{12}, ν_{21} and ν_{23}, where index 1 denotes axial direction, normal to the 23 plane.

2.4.2   Nonlinear Material Characterization with Reduced Order Model

In the nonlinear characterization, an undisclosed implicit analysis is performed by Multiscale Designer to test the fully nonlinear model. The solution algorithm, based on [10], is presented below.

> Initialize macro stiffness $\boldsymbol{C}$ and stresses $\boldsymbol{\sigma}$ for each Gauss point
> **for** *each macro solver increment* **do**
> Update macro stresses $\boldsymbol{\sigma}$
> **for** *each macro solver iteration* **do**
>   **for** *each macro Gauss point* **do**
>   Compute macro strains $\boldsymbol{\varepsilon} = \boldsymbol{C}^{-1}\boldsymbol{\sigma}$
>   **while** *not all phase strains* $\{\boldsymbol{\varepsilon}_{phase}\}$ *have converged* **do**
>   Compute phase strains $\{\boldsymbol{\varepsilon}_{phase}\}$ with model order reduction technique
>   Update phase stiffnesses $\{\boldsymbol{C}_{phase}\}$ based on nonlinear phase model and the damage and plasticity state
>   **end**
>   Update macro stiffness $\boldsymbol{C}$ and assign to Gauss point
>   **end**
> **end**
> **end**

To save computation effort, a model order reduction is implemented in the program. The main idea with this reduction is to compute micro strains $\boldsymbol{\varepsilon}^{phase}$ for every RVE phase directly from macro strains $\boldsymbol{\varepsilon}$. For this, phase strains are decomposed into elastic strains and eigenstrains, arising from inelastic deformation, thermal changes, moisture effects and oxidation. Further, a linear relation is assumed between micro and macro strains, for both elastic strains and eigenstrains. The linearity is represented by strain amplification matrices. Using this reduction, the approximate relation between micro strains and macro strains can be stated on the format of

$$\boldsymbol{\varepsilon}^{phase} = \boldsymbol{\varepsilon}^{phase}_{elastic} + \boldsymbol{\varepsilon}^{phase}_{eigen} = \boldsymbol{A}_{phase}\boldsymbol{\varepsilon}_{elastic} + \boldsymbol{P}_{phase}\boldsymbol{\varepsilon}_{eigen}$$

where $\boldsymbol{\varepsilon}^{phase}_{elastic}$ are phase elastic strains, amplified from macro elastic strains $\boldsymbol{\varepsilon}_{elastic}$ by the elastic strain amplification matrix $\boldsymbol{A}_{phase}$. Similarly, $\boldsymbol{\varepsilon}^{phase}_{eigen}$ are phase eigenstrains, amplified from macro eigenstrains $\boldsymbol{\varepsilon}_{eigen}$ by the eigenstrain amplification matrix $\boldsymbol{P}_{phase}$ [11]. Prior to the nonlinear analysis, these strain amplification matrices are computed

by undisclosed finite element simulations of the RVE. For these simulations, the RVE behavior is based on the linear material models assigned to each phase. Strain boundary conditions with only one non-zero component are applied, as in the linear characterization. Strain amplification matrices are only computed once, and can then be stored indefinitely for future nonlinear analyses of the same model [12], either in Multiscale Designer or in external CAE interfaces if the multiscale material is exported. The same strain amplification matrices can be used for any choice of nonlinear material model. Although the computation of strain amplification matrices carries a computation penalty, the total solution time is far shorter than for the opposed brute force approach; solving micro strains directly for each macro solver iteration [13]. For a full in-depth description of the reduced order model and general model order reduction, the reader is referred to [12].

2.4.3   Multiscale Material Model Export to CAE Interfaces

A finished multiscale material model can be exported to multiple CAE interfaces, e.g. Abaqus, Ansys and LS-Dyna, where it acts as a user defined material. In this work, the material model is integrated into Abaqus.

3   Method

A multiscale material model of paperboard is constructed based on X-ray images of paperboard. Used material models, and associated properties, are chosen to fit macroscopic experimental data as good as possible, given the constraints of the Multiscale Designer software. The multiscale modeling is carried through on a Windows operating system, as conditioned by Multiscale Designer.

To begin this section, the X-ray derived geometry is described. This geometry forms the basis of the definition of a representative volume element. Then a description is given for the characterization of linear and nonlinear material properties. The complete model is evaluated with virtual simulations. For more details regarding the modeling and simulation, see Appendix A.1.

3.1   X-ray Imaging and Definition of Representative Volume Element

An X-ray 3D scan is performed on a sample of single-ply paperboard. From the yielded image a small volume element is extracted, aiming to represent the macroscopical in-plane mechanical behavior of the paperboard. The volume element is discretized into solid 3D finite elements, with a 2 µm resolution to accurately capture the fiber geometry. Each solid element represents either fiber or air (the RVE must be completely meshed to function within Multiscale Designer). Thus, perfect bonding between fibers is assumed. To find an RVE with consistent model behavior, RVE:s with different sizes are tested. For this, fiber element sets are for sake of simplicity modeled isotropic, with stiffness 30 GPa and Poisson ratio 0.3. To motivate the need of an anisotropic model for in-plane calibration, an isotropic, rate independent plastic model is calibrated towards MD and simulated for both MD and CD. Given the need for an anisotropic model, a transversely isotropic model is evaluated. This is carried through by partitioning all fiber elements into disjunct element sets and assign one orientation to each set. For each set, a geometrical point within the set is chosen to evaluate the structure tensor, from which an approximate orientation vector is computed (for details, the reader is referred to [14]). This orientation vector defines the longitudinal direction of the transverse isotropy of the fiber. The effect of different number of orientations (and thus also fiber element sets) is investigated to further establish a consistent model behavior. The model consistency is measured with macroscopic properties; MD and CD elastic moduli E_x and E_y, and in-plane shear modulus G_{xy}. These moduli are obtained from Multiscale Designer. The size and number of orientations for a consistent RVE is assumed to yield consistency regardless of assigned material model.

3.2   Linear Material Characterization

In agreement with literature models of fiber (see [4] and [6]), fiber element sets are in this work modeled as transversely isotropic. The parameters describing this micromodel type are three moduli and two Poisson ratios. The moduli used are axial and longitudinal elastic moduli E_{11}^{fib} and E_{22}^{fib}, and in-plane shear modulus G_{12}^{fib}. The Poisson ratios used are out-of-plane, ν_{12}^{fib}, and in-plane, ν_{23}^{fib}. All fiber element sets are assigned identical parameter values. Air elements are modeled as isotropic, with properties given by Table 3. Parameter values to fiber and air elements are assigned, followed by a linear analysis in Multiscale Designer. This analysis is initiated in a batch file, with commands given by the Multiscale Designer user manual [15]. Due to limitations of the program, for this model the analysis has to be run in a forward motion, yielding macroscopic properties based on microscopic ones. The analysis is once again evaluated by comparing macro stiffnesses E_x, E_y and G_{xy} with experimental values. The analysis is rerun with different values of linear fiber parameters until a reasonably good fit against exper-

10

imental moduli is reached. The final fiber parameters are compared to those adapted in a similar transversely isotropic fiber model by [8]. To assess the spread of behavior for the established linear model, the model is assigned to 50 RVE:s, each created from different spatial positions within the X-ray sample. Each RVE is then run in a forward analysis, and the spread of yielded stiffnesses is measured.

As a necessary preparation for the nonlinear material characterization, reduced order model files are written for RVE:s on the established format. These model files will activate the model order reduction for the nonlinear simulations in Multiscale Designer. Note that these model files are based on a specific linear material model, with corresponding specific parameter values. Changing linear model type and/or parameter values without generating a new reduction file might decrease the accuracy and efficiency of the reduction.

3.3 Nonlinear Material Characterization

Air elements are modeled as completely linear elastic, with the same parameters as in the linear regime. For the fiber elements, only a few nonlinear material models are available, as conditioned by Multiscale Designer. In the context of this work, it is found that the best fit to experimental data is given by a isotropic linear hardening model. As previously mentioned, this choice of material model has been used in previous studies. For this model, the parameters are yield stress σ_0^{fib}, strain at ultimate stress ε_1^{fib} and strain to failure ε_2^{fib}. Additionally, Multiscale Designer needs the ultimate stress σ_1^{fib} as input. However, for easier model interpretation, the tangent stiffness E_t^{fib} is chosen instead. The ultimate stress is then computed as

$$\sigma_1^{fib} = \sigma_0^{fib} + E_t^{fib} \left(\varepsilon_1^{fib} - \left(\frac{\sigma_0^{fib}}{E_{11}^{fib}} \right) \right)$$

The fiber behavior is assumed symmetric in tension and compression. The resulting stress-strain curve is shown in Figure 3.
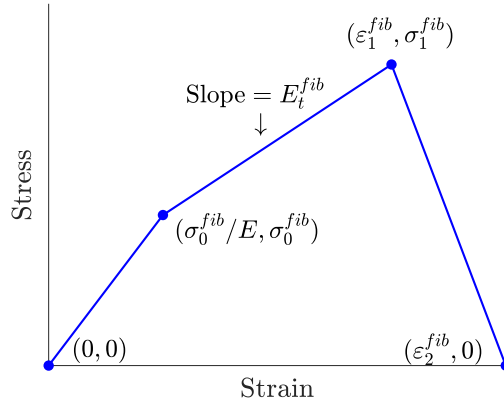
Figure 3: Stress-strain curve for the adapted nonlinear fiber model. For axial and transverse loading, the stiffness E takes values E_{11}^{fib} and E_{22}^{fib}, respectively.

With nonlinear parameters assigned to air and fiber element sets, a nonlinear analysis is run in Multiscale Designer. Similar to the linear analysis, the nonlinear analysis is initiated in a batch file, with commands given by the Multiscale Designer user manual [15]. As previously mentioned, this analysis is practically limited to a forward motion, due to limitations of the program for this model. The nonlinear analysis also enables common macroscopic simulations, one of which is uniaxial loading. Tensile tests are performed in MD, CD and 45 degree directions of loading, and the resulting stress-strain curves are compared with experimental data. The analysis is rerun with different values of nonlinear fiber parameters until a good fit against experimental moduli is reached. The final fiber parameters are compared to those adapted in a similar nonlinear elastic fiber model by [5]. To further evaluate the complete model, the σ_{11}-σ_{22} yield surface is computed, with uniaxial loading for multiple directions in the MD-CD-plane. Yield stress for each load case is defined as the stress at which 0.1 % plastic strain occurs.

3.4   Abaqus Simulations

The multiscale material model is exported into Abaqus where it acts as a user defined material. For these purposes, the continuum based material model developed by [16] (which has been previously validated) is used as comparison. In [16], a plate with a hole geometry under uniaxial tension is simulated (see Figure 4a) with dimensions $2L = 80$ mm, $2w = 50$ mm and $R = 10$ mm. Due to the symmetry, only a quarter of the geometry is considered for the simulation. The quarter plate is meshed into 1092 four-node plane stress elements (see Figure 4b). To reproduce the results from [16], two simulations are run: with either the material MD or CD parallel with the longitudinal direction of the plate. For the MD case, a displacement $u_x = 0.75$ mm is applied, whereas for the CD case, the displacement is $u_x = 1.25$ mm. In both cases, the largest principal Lagrangian strain is evaluated. To minimize solution divergence, the Riks

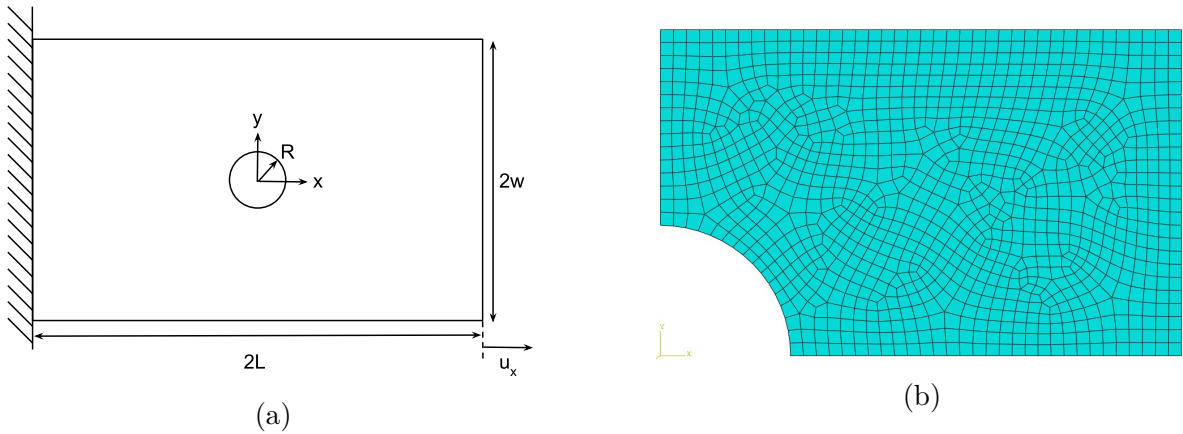path following algorithm is used with parameters given by Table 2.

Figure 4: a) Plate with a hole problem used for multiscale model evaluation. Due to the symmetry, only a quarter of plate is used for simulations. The quarter plate mesh is shown in b).

Table 2: Parameters for the Riks path following algorithm, used for the simulations in Abaqus [17].

Total arc length (-)	1.0
Initial arc increment (-)	10^{-4}
Minimum arc increment (-)	10^{-12}
Maximum arc increment (-)	1.0

4   Results and Discussion

4.1   RVE Analysis

To begin with, we study the size dependent response of the RVE as given by Figure 5a. The RVE size is measured with number of solid elements per RVE edge, where each element is 2 µm × 2 µm × 2 µm. There appears to be no clear convergence in macro stiffnesses as the RVE size is increased. At around size 40 sudden jumps in stiffnesses occur, perhaps due to a computational anomaly of some kind. Even larger RVE:s can be used, although with increased computation time. As an indication of time complexity for this analysis, the computation time is about 10 seconds for size 15, about 45 seconds for size 30 and about 600 seconds for size 50. To this end, RVE size might be a major modeling bottleneck, as it is currently unclear to what extent the Multiscale Designer analysis can be optimized for speed. As a compromise between computation accuracy and effort, a 30×30×30 element RVE format is chosen as a base for the modeling. Further, for the isotropic RVE:s tested, $E_x \approx E_y$ and $E_x \approx 2.5G_{xy}$, as given by Figure

5b. This is inaccurate as experiments suggest E_x should be at least 2 times larger than E_y and 4 times larger than G_{xy}. However, as proved by [2], it is possible to achieve macroscopic anisotropy with and isotropic fiber model. This approach, with a similar RVE size and resolution, was tested, but no distinct macroscopic anisotropy was yielded. An anisotropic material model therefore seems like a reasonable approach for this study. This is further suggested by Figure 6, where an isotropic material model will not yield reasonable fits in MD and CD simultaneously.
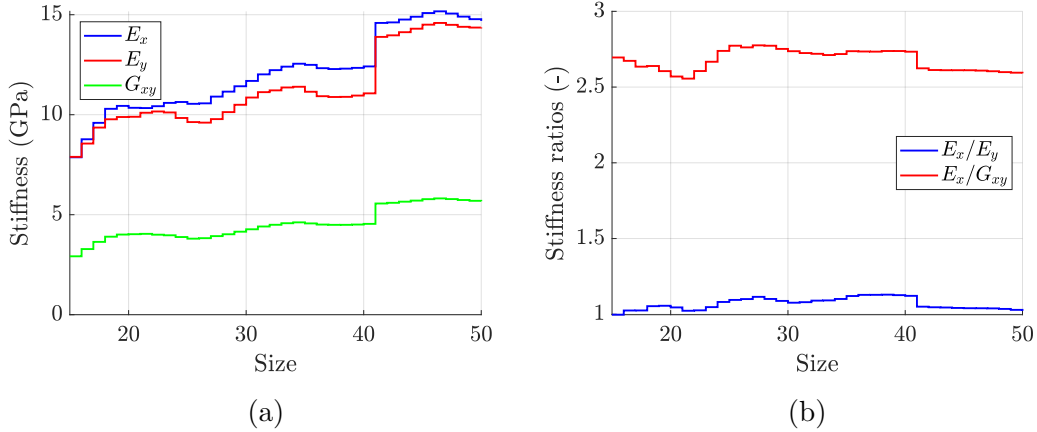

Figure 5: a) Macroscopic stiffnesses for different sizes of RVE:s used. The stiffnesses are obtained from Multiscale Designer. Size denotes number of solid elements per RVE edge, where each element is 2 µm × 2 µm × 2 µm. b) Stiffness ratios based on a).
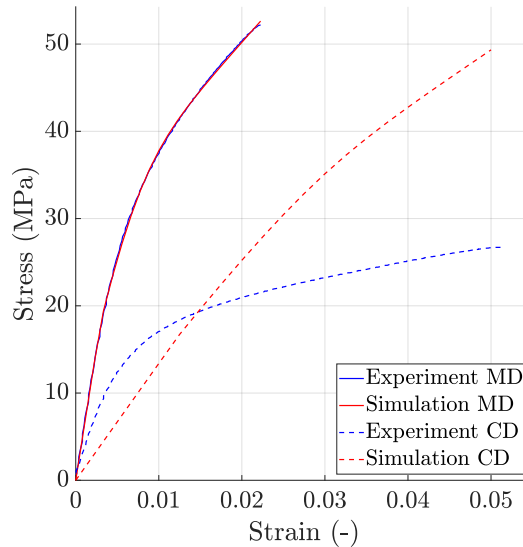

Figure 6: Stress-strain curves for an isotropic rate independent plastic material model under uniaxial loading. The model is calibrated for loading in MD, and the model response is shown for both MD and CD.

By choosing a transversely isotropic fiber model, we will consider how many different orientations should be used. Judging by Figure 7, there is a clear convergence in macro stiffnesses as the number of orientations are increased. This appears reasonable, since with more orientations, mainly oriented in MD, loads are carried in MD to a larger degree. Thus the response is stabilized. As the orientations are mainly in MD, i.e. in-plane, the in-plane shear response and stiffness is barely affected by the number of orientations used. There is no clear difference between using 26 or 212 orientations, indicating that assigning about 30 different orientations may be enough to obtain consistent RVE behavior.
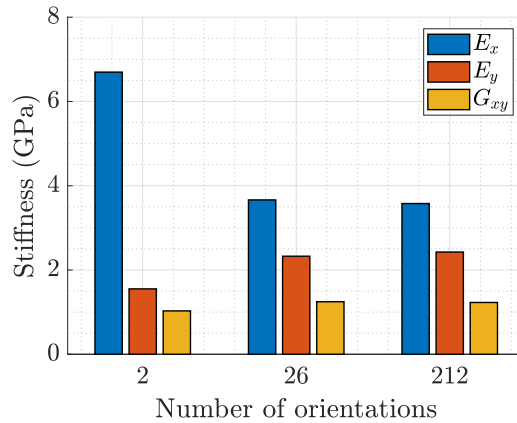

Figure 7: Macroscopic stiffnesses when using different number of orientations for transversely isotropic fiber element sets in the RVE. The stiffnesses are yielded from Multiscale Designer. Model parameters are as presented in Table 4.

A typical geometry of the RVE:s used is presented in Figure 8. Judging by this, the 2 µm resolution appears fine enough to capture individual paperboard fibers. One can distinguish a stacking of fibers in ZD, similar to the real life structure. Judging by the different ZD layers depicted in figures 9 a)-d), the fibers appear oriented mostly towards MD, with some alignment towards CD. It is important to capture both ZD stacking and MD dominated fiber orientation in the geometry, as it more accurately reflects the real life structure and therefore makes the calibrated model more relevant to use in simulations.
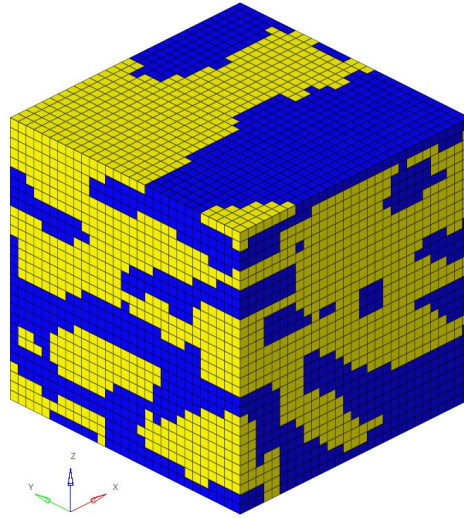
Figure 8: Typical geometry of the RVE:s used for modeling. The RVE consists of 30×30×30 elements, with each element being 2 µm × 2 µm × 2 µm. Fiber elements are colored yellow, air elements are colored blue.
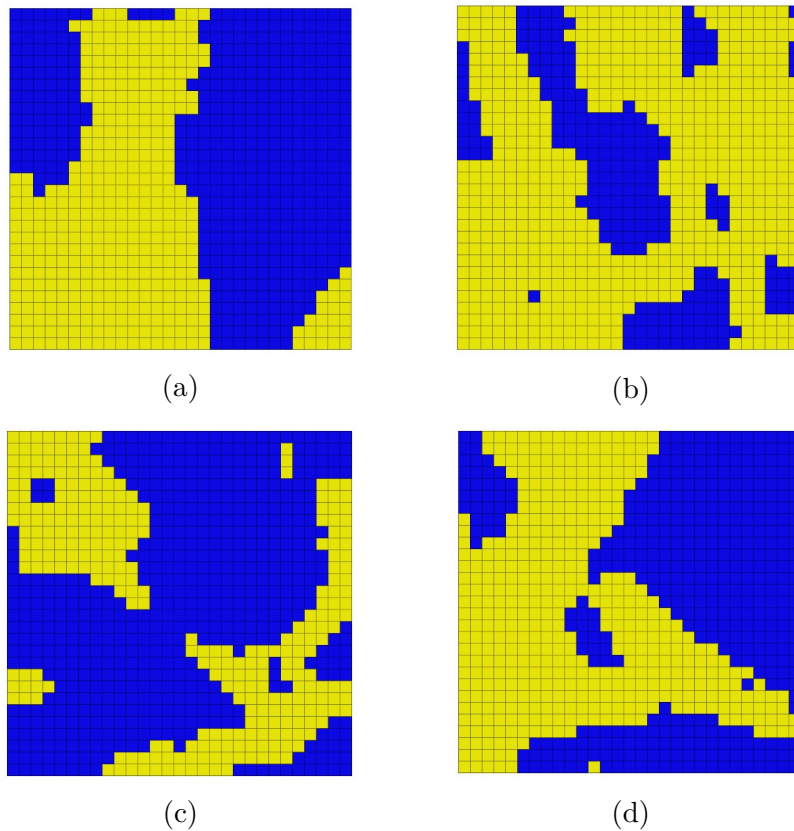

(a)

(b)

(c)

(d)

Figure 9: The same RVE as presented in Figure 8, viewed in the MD-CD-plane, with MD upwards and CD to the left. The views are equally spaced in the thickness direction, with (a) as the topmost layer and (d) as the bottommost layer (compare with Figure 8). Fiber elements are colored yellow, air elements are colored blue.

Another aspect which might influence the RVE behavior is boundary effects due to erroneous boundary conditions. However, it is found that whether the RVE is assigned periodic or fix boundary conditions (the only two BC:s applicable in Multiscale Designer), the model response is consistent. One may assume that the degree of periodicity for the RVE is large enough to justify a periodic assumption. To ensure strict periodicity, the RVE can be mirrored in 3D. However, this means only an eighth of the X-ray geometry can be captured for a constant RVE size (and computation effort). This approach, with retained RVE size, was tested briefly, and indicated a increased variability in macroscopic stiffnesses compared to non-mirrored RVE:s. One might assume higher model accuracy is obtained with larger, not completely periodic geometry, than with smaller, strictly periodic geometry.

The RVE does not capture two important mechanisms, which heavily influence the behavior of paperboard, particularly for large deformations. These mechanisms are fiber-fiber bond separation and friction between fibers sliding against each other. A conventional approach would be to include cohesive elements and surface interactions in the RVE, but, to this end, these features are not implemented and Multiscale Designer. Until these features have been implemented, cohesive and sliding effects could potentially be modeled with solid elements with suitable anisotropic properties.

4.2 Linear Material Characterization

The isotropic model of air is very simple. The air stiffness is set relatively close to the fiber axial stiffness (compare tables 3 and 4), to avoid numerical instability. This approach is also adopted by [2]. With high stiffness, air elements carry a relatively big fraction of the total load, and fiber stiffnesses must be erroneously reduced to decrease macroscopic stiffness and fit better with experimental data. Even so, the chosen fiber parameters, as presented in Table 4, are similar to those proposed by [6]. As fiber densities differ with only one order of magnitude, one can assume that the paperboard types calibrated against for both models are not too dissimilar. In the multiscale model there is a greater difference between axial and transverse fiber stiffness, relative to the model by [6]. This might be explained by the relatively few fibers captured within an RVE; for the few fibers captured, the anisotropy of the fibers has to be amplified to yield the target macroscopic anisotropy.

Table 3: Numerical values of linear elastic air properties. In SI units the density value is 1.29 kg/m³.

Material parameter	Value
E (GPa)	2.0
ν (-)	0.3
ρ (tonnes/mm^3)	$1.35 \cdot 10^{-12}$

Table 4: Numerical values of linear elastic fiber properties, for the multiscale model and for a similar transversely isotropic fiber model by [6]. The Poisson ratios have no major impact on the RVE behavior and are therefore set as zero. For the multiscale model, the density value is 90 kg/m^3 in SI units.

Material parameter	Multiscale model	Brandberg et al 2020 [6]
E_{11}^{fib} (GPa)	30	30
E_{22}^{fib} (GPa)	0.75	3.0
G_{12}^{fib} (GPa)	2.0	3.0
ν_{12}^{fib} (-)	0	0
ν_{23}^{fib} (-)	0	0
ρ^{fib} (tonnes/mm^3)	10^{-10}	$1.58 \cdot 10^{-9}$

Given the fiber model in Table 4, the RVE behavior appears consistent. Across the 50 transversely isotropic RVE:s tested, solidity (volume fraction of solid material) ranges between 43 % and 72 %. Despite this variability, macro stiffnesses do not spread more than 20 %, as seen in Table 5. The solidity dependence of stiffnesses is most prominent in MD, causing a greater variability compared to CD stiffness. The in-plane shear stiffness varies only 6 % due to the weak solidity dependence. Also, the simulated stiffnesses are relatively close to experimental ones. An even better calibration can be achieved with more analysis iterations. Due to time constraints, this is not considered in this work.

Table 5: Macroscopic stiffnesses and spread of these parameters across the 50 simulated RVE:s. The stiffnesses are yielded from Multiscale Designer.

Macro stiffness	Mean value (GPa)	Coeff. of variation (-)	Experimental value (GPa)
E_x (GPa)	5.47	0.20	6.60
E_y (GPa)	3.03	0.14	3.06
G_{xy} (GPa)	1.51	0.06	1.63

4.3   Nonlinear Material Characterization

For each RVE used in the nonlinear analysis, the generation of model order reduction files took about 90 minutes. As previously mentioned, this computation penalty is worth taking, as the model order reduction allows for drastically shorter simulation times.

As seen in Table 6, the multiscale model applies a fiber model with lower yield stress and less hardening compared to the isotropic hardening model developed by [5]. It is possible that the geometry of RVE:s used amplifies the plastic stiffness, which has to be compensated with the model parameters. Still, the set of parameters yield reasonable fits for MD, CD and 45 simultaneously, as seen in Figure 10a, 10b and 10c. It is found that, by changing model parameter values, the response in CD is most affected, followed by the 45 degree direction and MD. Thus, the CD response to some degree conditions the response in MD and 45 degrees. For each load case, the three different simulations all behave similarly and do not spread too much, which is a further sign of consistent RVE behavior. Some erratic oscillations occur when loading in 45 degrees (Figure 10c) and, more prominently, in CD (Figure 10b). These oscillations are not caused by failure of fiber element sets, as the oscillations persist even when the strains at ultimate stress and failure are set arbitrarily large, prolonging the failure regime. This is then likely a case of material instability. As the material is weakest in CD it makes sense that material instability arises most prominently in this direction. Another sign of unstable response in CD is the onset of plasticity, which is very sudden compared to 45 degrees and MD.

Table 6: Numerical values of nonlinear fiber properties, for the multiscale model and for a similar isotropic hardening model by [5]. The model in [5] does not consider damage accumulation.

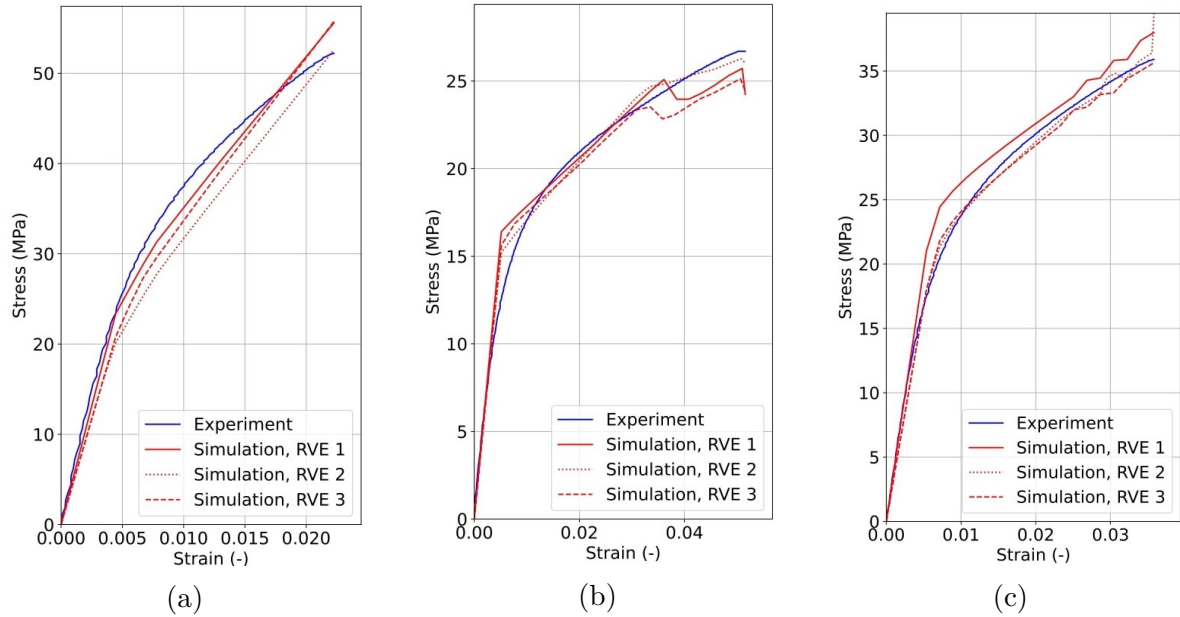| Material parameter	Multiscale model	Borodulina et al 2016 [5]
Yield stress σ_0^{fib} (MPa)	65	150
Tangent stiffness E_t^{fib} (GPa)	0.3	10
Strain at ultimate stress ε_1^{fib} (-)	0.2	-
Fracture strain ε_2^{fib} (-)	0.2	-

Figure 10: Stress-strain curves for uniaxial loading in MD (a), CD (b) and 45 (c) degree direction, experimental and simulated for three different RVE:s.

Another important model aspect is that failures do not occur at the points measured experimentally. It is extremely difficult to calibrate the model such that it captures both the nonlinear response and failure point in MD, CD and 45 degrees simultaneously. With model parameter values according to Table 6, failure strains are found to be roughly 3.5 %, 9 % and 6 % in MD, CD and 45 degrees, respectively (i.e., in Figure 10, the model is yet to fracture). These strains are larger than in experiments, although the ratios between these strains are similar to those in experiments. To conclude, the nonlinear response is prioritized, at the sacrifice of inaccurate failure points. Thus, the model may not be used to predict material failure.

On an additional note, other nonlinear material models available in Multiscale Designer have been tested. A fiber damage model allegedly captures the complex compressive failure of fibers, and is linear elastic in tension until a sudden failure. For the RVE:s tested, this model yields a very good fit in MD, but plastic softening in CD and practically ideal plasticity in 45 degrees, regardless of parameters used. This model may be considered for modeling of compressive load cases, where the real material response is very different in character compared to tensile loading. Moreover, an orthotropic hardening plasticity model has also been tested. For the RVE:s tested, this model carries an immense computational effort. Runtimes are at least an hour long, even when parameters are chosen such that the hardening becomes isotropic. It remains to be examined whether or not the model accuracy for tensile loading is higher for orthotropic plasticity than for isotropic plasticity.

As the macroscopic model response agrees well with experimental data, the model fulfills its purpose. This is further solidified by Figure 11, showing similarities between the yield surfaces given by the multiscale model and continuum based model in [16]. Both surfaces can be crudely approximated as rounded squares, and stresses are in similar ranges. This also justifies the multiscale model as a base for further model development.
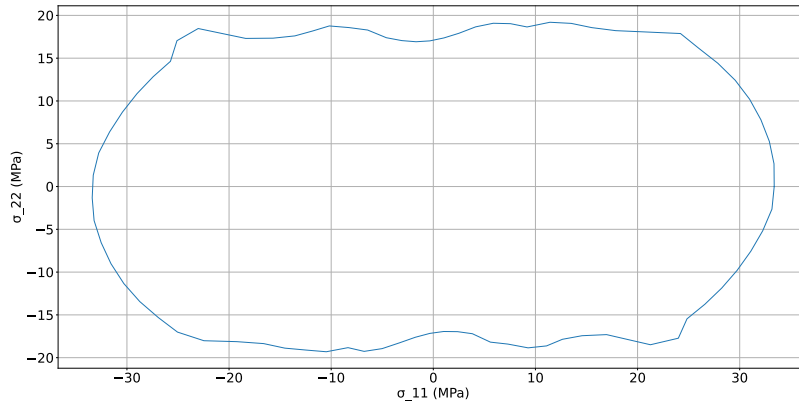
(a)
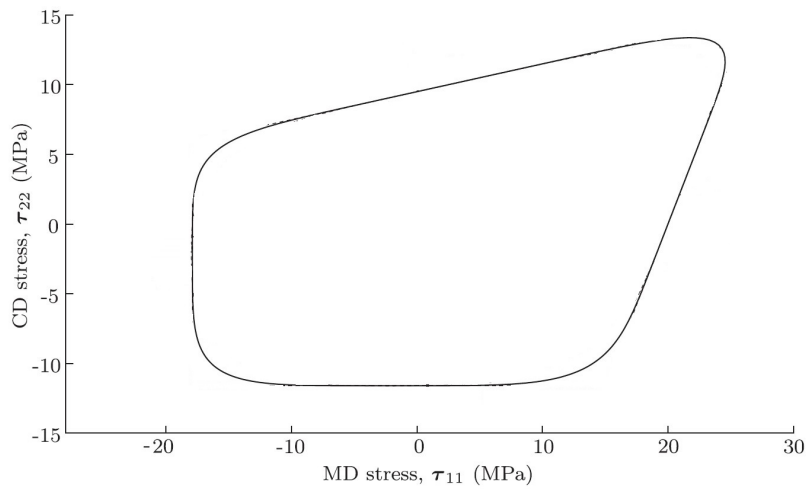
(b)

Figure 11: Simulated yield surfaces; a) in the σ_{11}-σ_{22} plane as derived from the multiscale model, b) in the τ_{11}-τ_{22} plane as presented in [16] (reworked). Note that different types of stress measures are used. This makes the different stresses differently scaled to some degree, but does not affect the shapes of the yield surfaces.

4.4   Abaqus Simulations

The Abaqus simulations do not perform as intended, as the finite elements become heavily distorted before the full loads are applied. Thus, the maximum simulated loads are 0.41 mm and 0.14 mm for MD and CD respectively. This erroneous behavior can be explained neither with the load increment size, as this is kept relatively small, nor with material failure, as the model fails at larger strains than shown experimentally. A more likely explanation is material instability, as previously discussed. Still, even with lower load levels than intended, there are some similarities between the strain fields produced in this work and by [16]. The best agreement is in MD, as shown in Figure 12, where the strain field distribution is very similar between 12a and 12b. With comparable load levels, the maximum strain in 12a is 3 times greater than in 12b. This is a relatively good agreement considering the relative simplicity and black box character of the multiscale model. There is a greater discrepancy in Figure 13, where maximum strains are higher in 13a than 13b despite five times lower displacement load. Also, strains are more localized in 13a than in 13b. It is unclear if a equal load levels would yield similar strain field distributions, as in Figure 12. Still, the similarities between the models are promising for further development of the multiscale model.
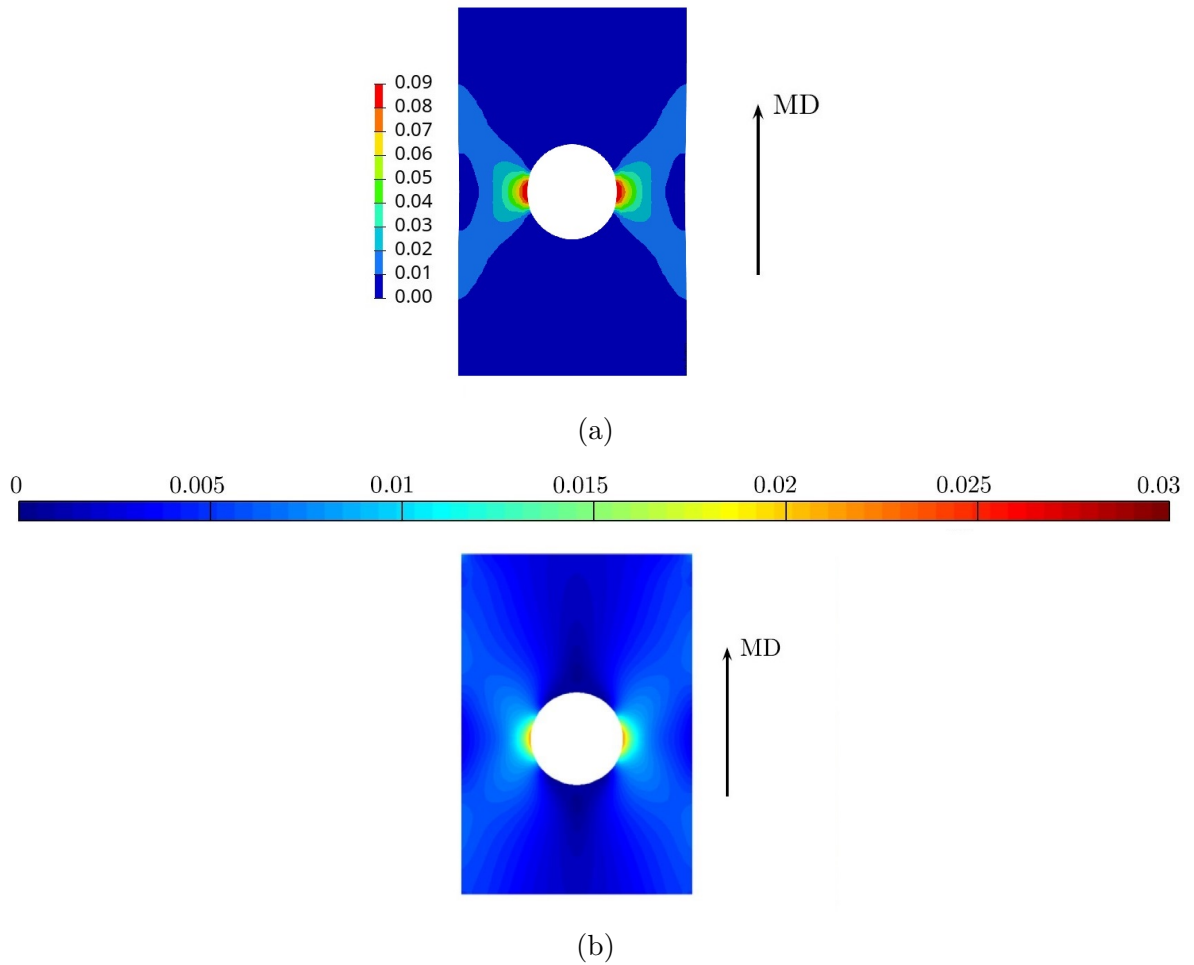
(a)

(b)

Figure 12: Largest principal Lagrangian strain for the plate with a hole problem, when the material MD is parallel with the longitudinal direction of the plate. (a) Multiscale material model simulation (0.41 mm displacement load), (b) Continuum based material model simulation from [16] (0.45 mm displacement load) (reworked).
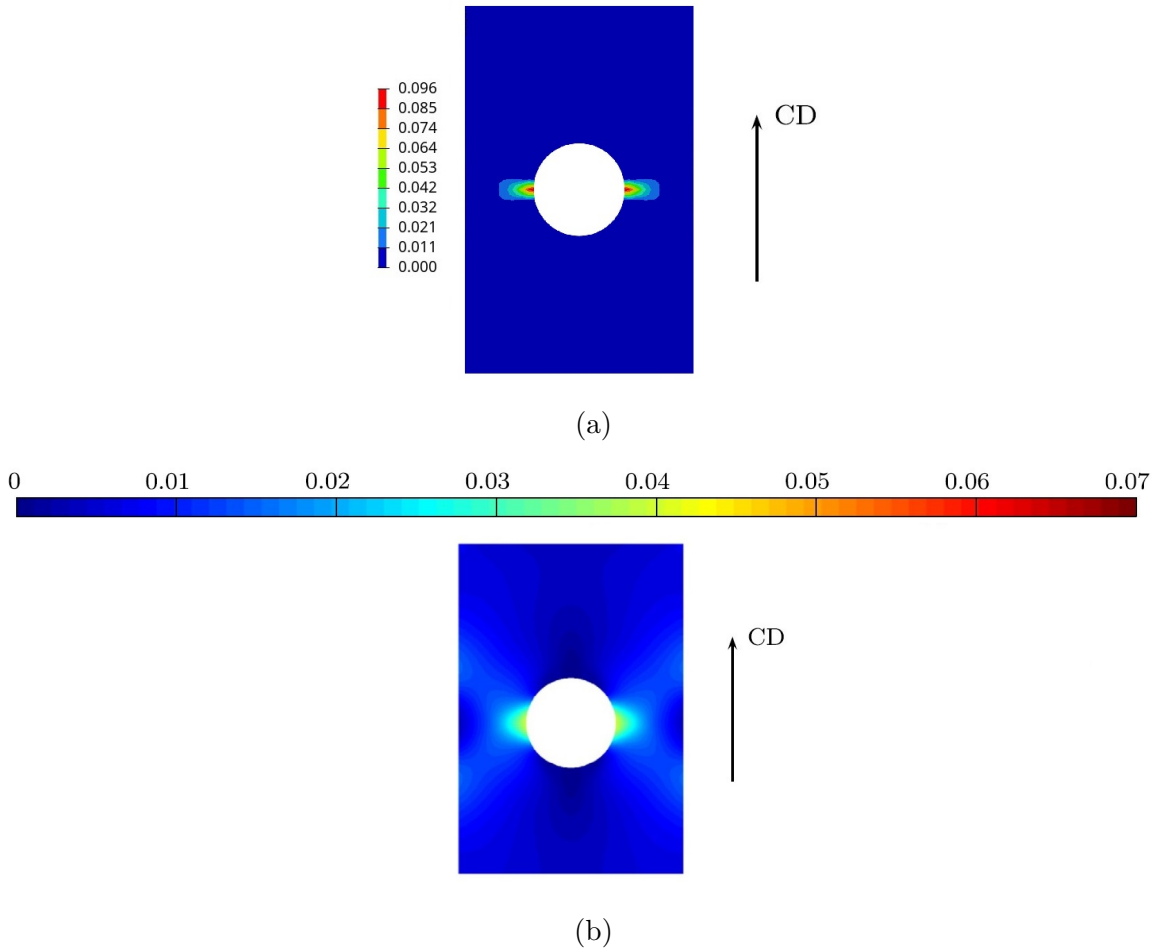
(a)

(b)

Figure 13: Largest principal Lagrangian strain for the plate with a hole problem, when the material CD is parallel with the longitudinal direction of the plate. (a) Multiscale material model simulation (0.14 mm displacement load), (b) Continuum based material model simulation from [16] (0.75 mm displacment load) (reworked).

4.5   Multiscale Modeling Workflow

As the multiscale model appears reasonably accurate for in-plane uniaxial tensile loads, the workflow may be discussed. It turns out that a large part of the modeling can be automatized, with text files written based on the material model chosen, and used as input in the linear and nonlinear analyses, which are called by batch file commands. The main challenge is to understand the function of each text file, and ensure it contains the desired model information in a correct format, as conditioned in the Multiscale Designer manual [15]. It is particularly important to correctly implement the file containing RVE mesh data, as this forms the base of the multiscale model. Given a material model, different parameter values can easily be tested in a forward analysis manner. Hopefully, future versions of Multiscale Designer will also allow inverse characterization for models similar to this work. Alternatively, one might try to self implement an external inverse

optimization function.

Within the time frame of this work, it is found that Abaqus simulations with multiscale materials are difficult to fine-tune and automatize. The basic steps required to get such simulations to run at all have been established, but more work needs to done to achieve a smoother integration into more complex simulations.

4.6 Future Work

This project shows that accurate multiscale modeling of paperboard is possible, using Multiscale Designer. Whether or not more complex and accurate models can be built is a matter of implementation limits in the software. Ideally, one would like to capture paperboard behavior at additional and more complex load cases. It would also be interesting to see how the model behavior changes by implementing fiber-fiber bonds, as these heavily influence the real material response. Other possible factors to consider are temperature and moisture dependency.

Retaining the objective of in-plane model calibration, it would be interesting to further investigate how the model behavior changes if a non-equilateral RVE is used. This was briefly tested when trying to reproduce the results by [2]. For in-plane calibration, it seems likely that a fine in-plane resolution and coarse ZD resolution would increase model accuracy.

Further, it would be interesting to obtain a more reasonable behavior when the multiscale model is integrated into an Abaqus simulation. Then, it would be interesting to do a more detailed comparison between the multiscale modeling approach and conventional continuum based models. For this comparison one might use field output for each element set defined in the model. This output is provided by Multiscale Designer. Using this, quantities such as plastic strains and damage parameters may be localized within the model.

Another interesting aspect is trying to apply the methodology of this work for multiscale analysis of other types of paper, e.g. writing and printing paper.

5 Conclusions

To summarize this thesis, it is concluded that it is possible to create a reasonably accurate multiscale material model of paperboard, and capture the experimental behavior at in-plane uniaxial tensile loads. This model consists of a bi-phase RVE, with fiber and air phases. Perfect fiber-fiber bonding is assumed. The fibers are modeled as transversely isotropic elastic in the linear regime, and with isotropic hardening in the nonlinear regime. A model behavior regarded as consistent is given by an RVE with $30{\times}30{\times}30$ solid 3D elements, 2 µm resolution and at least 30 orientations defined for the transversely isotropic fiber element sets. The model is reasonably accurate for nonlinear deformations, although it fails at predicting material failure points.

The model can also be exported as a user material in Abaqus. As a model evaluation, simulations are performed to compare the multiscale model with a previously established continuum based model. Strain fields for the different models are used for comparison. Although these fields differ, there are some similarities, which is promising for further model development.

The multiscale modeling workflow can be automatized to some degree. For this, one needs to ensure the correct content and format of text files used as input in the modeling analyses.

In future works one can consider more complex models, calibrated towards additional and more complex load cases.

References

[1] Y. Li et al. Evaluation of the out-of-plane response of fiber networks with a representative volume element model. *Tappi Journal*, 2018.

[2] M. Nygårds & E. L. Bonnaud. Network modeling of paper materials: a micromechanical model to investigate the influence of fiber properties. 2010.

[3] J. Tryding. *In-plane fracture of paper*. PhD thesis, Lund University, Division of Structural Mechanics, 1996.

[4] K. Persson. *Micromechanical Modelling of Wood and Fibre Properties*. PhD thesis, Lund University, Division of Structural Mechanics, 2000.

[5] S. Borodulina et al. Effect of fiber and bond strength variations on the tensile stiffness and strength of fiber networks. *International Journal of Solids and Structures*, 2016.

[6] A. Brandberg et al. The role of the fiber and the bond in the hygroexpansion and curl of thin freely dried paper sheets. *International Journal of Solids and Structures*, 2020.

[7] A. Brandberg & A. Kulachenko. The effect of geometry changes on the mechanical stiffness of fiber-fiber bonds. *Advances in Pulp and Paper Research*, 2017.

[8] A. Brandberg & A. Kulachenko. Compression failure in dense non-woven fiber networks. *Cellulose*, 2020.

[9] L. Xing et al. A new stress-based multi-scale failure criterion of composites and its validation in open hole tension tests. *Chinese Journal of Aeronautics*, 2014.

[10] F. Ehrhart. Multiscale designer basic training. Digital training course, 2021.

[11] J. Wollschlager et al. A technical overview of altair multiscale designer. *International Journal for Multiscale Computational Engineering*, 2021.

[12] J. Fish. *Practical Multiscaling*. John Wiley & Sons, 2014.

[13] G.M.K. Pearce et al. Strain invariant failure theory – part 1: An extensible framework for predicting the mechanical performance of fibre reinforced polymer composites. *Composite Structures*, 2019.

[14] R. M. Auenhammer et al. X-ray computed tomography data structure tensor orientation mapping for finite element models — STXAE. *Software Impacts*, 2022.

[15] *Altair Multiscale Designer User Manual*, 2021.

[16] E. Borgqvist et al. Distortional hardening plasticity model for paperboard. *International Journal of Solids and Structures*, 2014.

[17] *Dassault Systemes Abaqus User Manual*, 2021.

A   Appendix
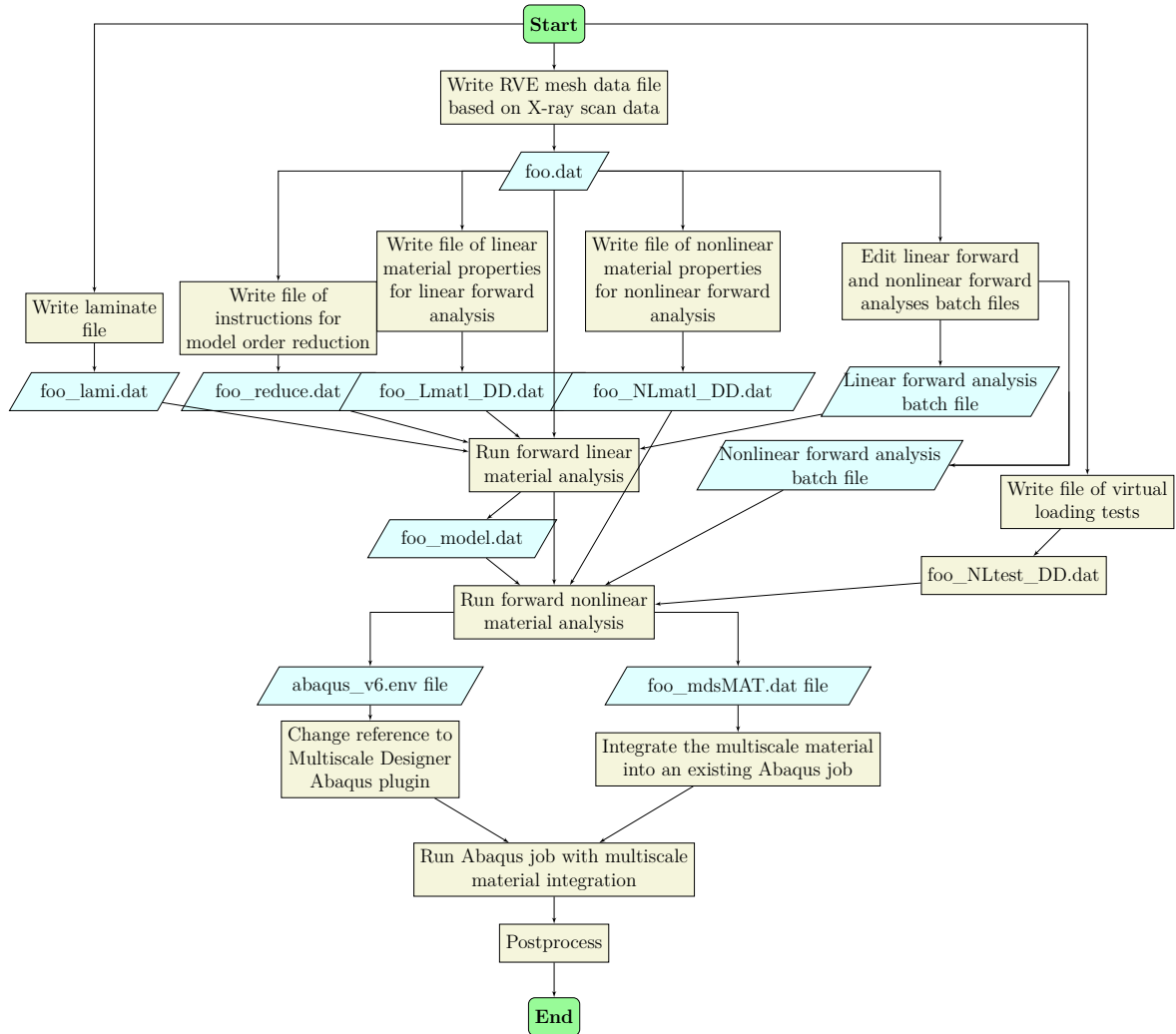
A.1   Summary of Workflow

Figure 14: Summarizing flowchart for the multiscale modeling workflow of this work. The input files required for the linear and nonlinear analyses are created, whereafter the analyses are performed. The output files of the analyses are integrated into an existing Abaqus job where homogeneous materials can be replaced with the yielded multiscale material. The file `foo_model.dat` contains the elements of the strain amplification matrices $\boldsymbol{A}_{phase}$ and $\boldsymbol{P}_{phase}$ for each phase in the RVE. This file only needs to be created once.